Review of Scientific Instruments

Ensemble-statistical approach in the measurement of air–water flow properties in highly unsteady breaking bores

Cite as: Rev. Sci. Instrum. **93**, 054502 (2022); https://doi.org/10.1063/5.0077774
Submitted: 06 November 2021 • Accepted: 29 April 2022 • Published Online: 25 May 2022

Davide Wüthrich, Rui Shi and Hubert Chanson

AIP Publishing

Review of Scientific Instruments ARTICLE scitation.org/journal/rsi

Ensemble-statistical approach in the measurement of air–water flow properties in highly unsteady breaking bores

Cite as: Rev. Sci. Instrum. 93, 054502 (2022); doi: 10.1063/5.0077774
Submitted: 6 November 2021 • Accepted: 29 April 2022 •
Published Online: 25 May 2022

Davide Wüthrich[1,2,a)] Rui Shi,[2,b)] and Hubert Chanson[2,c)]

AFFILIATIONS

[1] Department of Hydraulic Engineering, Delft University of Technology, 2628 CN Delft, The Netherlands
[2] School of Civil Engineering, The University of Queensland, Brisbane, QLD 4072, Australia

[a)] **Author to whom correspondence should be addressed:** d.wuthrich@tudelft.nl
[b)] **Email:** rui.shi@uq.net.au
[c)] **Email:** h.chanson@uq.edu.au

ABSTRACT

Breaking bores are commonly observed in a number of natural processes, often associated with the presence of a transient mixture of air and water, with intense recirculation, air bubble entrainment, and splashing. Two-phase flow measurements in such highly unsteady flows cannot be based on long-duration measurements and require novel ensemble-statistical approaches based on multiple repetitions. Detailed measurements of air–water flow properties were then conducted in a breaking bore with Fr_1 = 2.4 using an array of multiple dual-tip phase-detection probes. Based on an extensive experimental program, inclusive of 2000 tests at a single position and 100 tests at multiple elevations, a detailed sensitivity analysis was conducted on the necessary number of repetitions to obtain physically meaningful and statistically reliable air–water flow properties. The results led to a robust methodology to estimate ensemble-statistical values, including confidence intervals and residual error. In addition, these results provided a detailed characterization of the behavior of air–water flow properties in highly unsteady flows, including void fraction, number of interfaces, and bubble chord time/length. Despite the transient nature, all physical processes showed consistent behaviors with theoretical models and other stationary flows, including hydraulic jumps and plunging jets. Overall, this study provided two-phase flow characteristics that go beyond the limitations imposed by the unsteady nature of the flow, proving thoroughly the importance of large datasets for the estimation of air–water flow properties in highly unsteady flows.

I. INTRODUCTION

The unsteady propagation of breaking bores is commonly observed in nature during flood events, coastal processes, man-induced rejection surges, tidal bores, and tsunamis propagating in rivers. These flow conditions are often associated with the generation of a breaking roller with a recirculating pattern and large air entrainment (Tricker, 1965). Aeration is responsible for substantial changes in flow properties, relevant in a number of environmental processes, including the impact on natural and man-made structures (Chanson, 2011; Wüthrich *et al.*, 2018). In coastal and maritime processes involving breaking waves interacting with coastal structures, Bullock *et al.* (2001) showed that air modifies impact pressures, affecting the dynamics of the loads. Thus, a comprehensive quantification of their air–water flow properties in highly unsteady breaking bores is fundamental.

Air–water flow properties were widely investigated in steady flows, including hydraulic jumps, smooth and stepped spillways, and plunging jets. Intrusive instruments capable of investigating air–water phases include optical fiber probes (Cartellier, 1992; Chang *et al.*, 2003) and conductivity probes (Chanson, 2004a). In steady flows, the computation of air–water flow properties is based on long-duration measurements and time averaging, for which previous sensitivity analyses recommended a minimum duration of 45 s and an acquisition frequency of 20 kHz (Chanson, 2007a; Chanson and Felder, 2010; and Wüthrich and

Chanson, 2014). Contrarily, because of their transient nature, little attention was given to air–water flow properties in unsteady flows, with the exception of few earlier contributions by Cox and Shin (2003), Chanson (2004c), Hoque and Aoki (2005), Kimmoun and Branger (2007), Blenkinsopp and Chaplin (2007; 2011), Mori and Kakuno (2008), Na *et al.* (2016), Leng and Chanson (2019b; 2019a), and Wüthrich *et al.* (2020a). The highly transient nature of these flows complicates the acquisition of reliable long-duration data, unless performing a large number of repetitions to compute ensemble statistics (Bradshaw, 1971; Schlichting and Gersten, 2001; and Docherty and Chanson, 2012). These statistical results are highly dependent on the number of repetitions, implying that an insufficient dataset will result in high scatter or unreliable results. Previous results on unsteady bores showed that at least 20 repetitions were necessary for accurate measurements of free-surface properties, velocity components, and tangential stresses in clear-water flows (Leng and Chanson, 2017; Chanson, 2020).

However, to date, no sensitivity analysis was ever performed on the number or repetitions necessary to obtain meaningful and reliable air–water properties in unsteady flows. This implies that little knowledge is available on the behavior of air–water flow properties in breaking bores and the physical processes associated with these transient flows remain widely not understood. In this context, the present study has the double objective of (1) discussing the effect of the number of repetitions on the estimation of ensemble-statistical air–water flow properties, including confidence intervals and residual error, and (2) providing a detailed description of their variation in both space and time, in support of a better understanding of the physical processes associated with highly unsteady breaking bores.

II. EXPERIMENTAL SETUP AND FLOW CONDITIONS

All tests were performed at the University of Queensland in a 19 m long rectangular tilting channel with a width of 0.7 m and a depth of 0.5 m. Bores were generated through the sudden closure of a Tainter gate, inducing a positive surge advancing in the upstream direction. An inflow discharge $Q = 0.099$ m^3/s was tested for two channel slopes $S_0 = 0.75\%$ and 1.25%, resulting in breaking bores with Froude numbers $Fr_1 = 2.1$ and 2.4, respectively. The characteristics of the initially steady flows and the bore main properties are detailed in Table I. In agreement with previous studies, all measurements were taken at $x = 8.5$ m from the channel inlet, where the bores were fully developed. The air–water flow properties were measured by means of two double-tip phase-detection conductivity probes: a reference probe and a center probe (Fig. 1). Both were manufactured with silver inner electrodes ($Ø = 0.25$ mm) and stainless-steel outer electrodes ($Ø = 0.8$ mm), with a transversal distance between the tips of $\Delta y = 1.8$ mm, and all leading tips were located at the same streamwise location $x = 8.5$ m. The reference probe was installed at $y = 0.30$ m from the sidewall ($y/W = 0.43$) and had two leading tips (i.e., $\Delta x = 0$ mm), while the center probe was located at $y = 0.35$ m ($y/W = 0.50$) and had a leading and a trailing tip with $\Delta x = 6.3$ mm. For both probes, the signal was acquired at $f = 100$ kHz.

TABLE I. Flow conditions and experimental program. Note the following parameters: Fr_1 is the Froude number, Q is the water discharge, S_0 is the slope of the invert, d_1 is the initial still water depth, V_1 is the initial flow velocity, U is the bore front celerity, f is the acquisition frequency, z is the vertical elevation, y is the transversal distance, and W is the channel width ($W = 0.7$ m).

Dataset	Fr_1	Q (m^3/s)	S_0 (%)	d_1 (m)	V_1 (m/s)	U (m/s)	f (kHz)	z (m)	y/W	Repetitions n
1	2.4	0.099	1.25	0.084	1.707	0.504	100	0.089	0.43	2000
2	2.4	0.099	1.25	0.084	1.707	0.504	100	0.069–0.239 (20 elevations)	0.50	100
3	2.1	0.099	0.75	0.097	1.468	0.627	100	0.113	0.50	100
	2.1	0.099	0.75	0.097	1.468	0.627	100	0.163	0.50	100

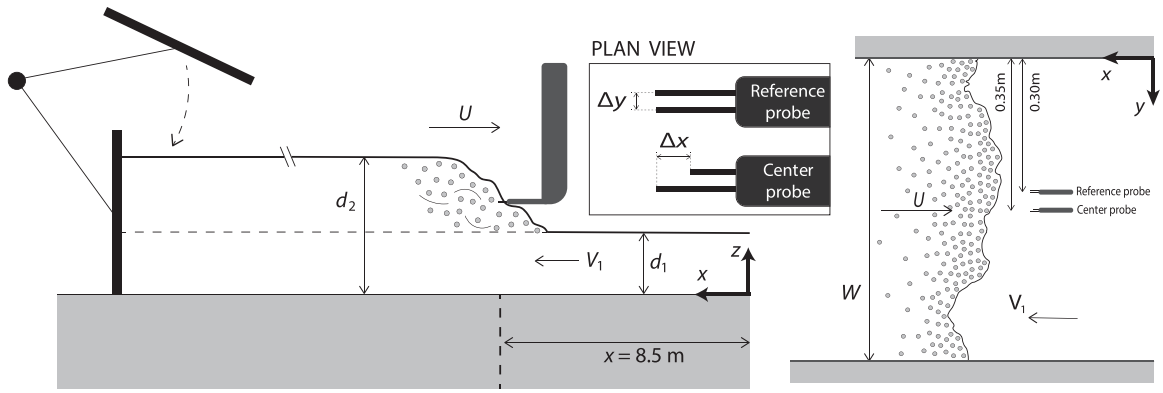

FIG. 1. Experimental setup and details of the phase-detection conductivity probes.

The reference probe was sampled for 2000 repetitions at the same elevation $z = 0.089$ m ($z/d_1 = 1.06$), while the center probe was sampled at 20 elevations (0.069 m < z < 0.239 m), each for 100 repetitions (Table I). This generated two complementary datasets, allowing us to conduct a detailed sensitivity analysis with a large number of repetitions at one elevation (dataset 1: $Fr_1 = 2.4$, reference probe with 2000 tests) and verify these results for a number of elevations in the bore (dataset 2: $Fr_1 = 2.4$, center probe with 100 tests at 20 elevations). In addition, a third dataset was collected with the center probe for a Froude number $Fr_1 = 2.1$ at two selected elevations: $z = 0.113$ and 0.163 m ($z/d_1 = 1.16$ and 1.68, respectively), with identical flow conditions to Leng and Chanson (2019b; 2019a). Three Acoustic Displacement Meters (ADMs), microsonic-type mic+35/IU/TC, were used to detect the water depth at $x = 7.0$, 8.5, and 10 m, with an emission frequency of 400 Hz and a response time of 64 ms. These allowed us to measure the mean bore front celerity as the ratio of sensors' distance over traveling time. The experimental program is summarized in Table I.

III. SIGNAL PROCESSING AND METHODOLOGY

Two main techniques were applied to convert the raw voltage signal captured by the phase-detection probes to the instantaneous void fraction with values of 0 (water) and 1 (air).

1. The **single threshold (ST) technique** [Fig. 2(a)] set at 50% of the voltage difference between air and water (Cartellier and Achard, 1991) has been widely used in previous studies on air–water flow properties, mostly applied to stationary flows, such as partially filled conduits (Chanson, 1997a), supercritical open channel flows (Chanson, 1997b), water jets (Brattberg *et al.*, 1998), hydraulic jumps (Wang, 2014), stepped spillways (Chanson and Toombes, 2002; Gonzalez, 2005), and unsteady flows (Chanson, 2004a; 2004b; and 2004c). A drawback of the single threshold technique is that it does not detect small events that do not reach 50% of the voltage difference between air and water.
2. The **linear threshold (LT) technique** [Fig. 2(b)] was recently employed by Leng and Chanson (2019b; 2019a) and Wüthrich *et al.* (2020b) for unsteady bores. It was implemented because it is more sensitive to small air–water entities and fast transient interfacial processes, as it allows us to detect events that are neglected with the single threshold technique. In Fig. 2(b), the linear threshold technique assumed a linear variation between the air phase (v_{min}) and the water phase (v_{max}), proportional to the voltage measured by the phase-detection probe. To avoid the adverse influence of signal noise, herein the linear variation was assumed between $v_{min} + 0.1\Delta v$ and $v_{max} - 0.1\Delta v$, where $\Delta v = v_{max} - v_{min}$.

From the air–water signal, a number of parameters could be obtained. An **interface** was defined as an individual phase change, either water-to-air or air-to-water. With both single and linear threshold techniques, it was defined as an overstep of the value $0.5 \cdot \Delta v$. The total number of interfaces was even for $z < d_1$ and odd for $z > d_1$. The number of bubbles b is, therefore, defined as

$$b = \frac{N - \xi}{2} \text{ with } \begin{cases} \xi = 0 & \text{for } z < d_1, \\ \xi = 1 & \text{for } z > d_1. \end{cases} \quad (1)$$

For every bubble, its **chord time** t_{ch} was computed as the duration between the water-to-air interface and the subsequent air-to-water interface, corresponding to the value of $0.5 \cdot \Delta v$. The **pseudo-chord length** was deduced, assuming a constant propagation speed equal to the bore front celerity U,

$$L_{ch} = U \cdot t_{ch}. \quad (2)$$

Herein, all bubbles whose chord time was $t_{ch} < 0.000\,15$ s (i.e., $L_{ch} = U \cdot t_{ch} = 7.96 \cdot 10^{-5}$ m) were rejected, as these were considered physically meaningless.

For stationary flows, the time-averaged **void fraction** is defined as the average time spent in air relative to the total duration of the signal. From a statistical perspective, this corresponded to the probability of the sensor's tip to be located in air. For breaking bores, long-duration measurements were physically meaningless because of the non-stationary nature of the flow. Instead, a large number of

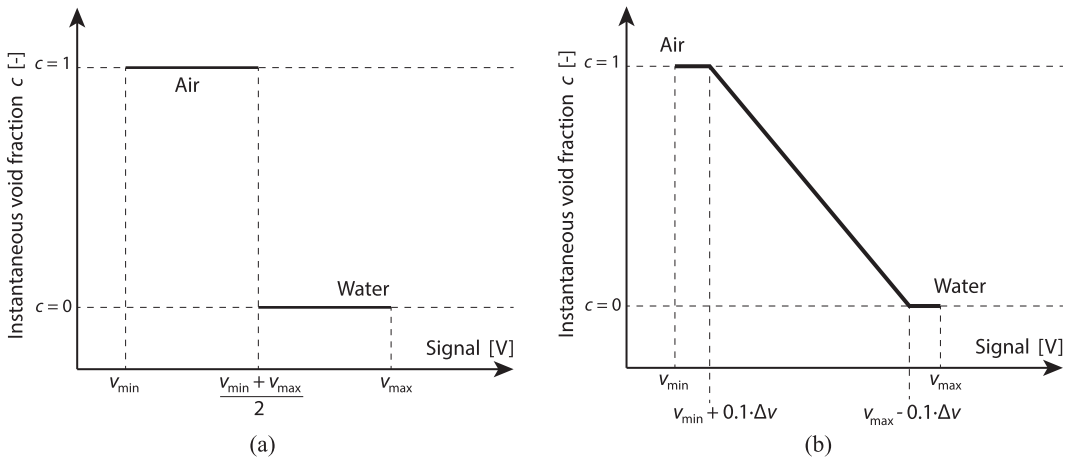

FIG. 2. Conversion techniques from a raw voltage signal to an instantaneous void fraction: (a) single threshold technique and (b) linear threshold technique.

repetitions were conducted and data analyzed in terms of ensemble-statistical properties. This approach required good repeatability of the experimental tests with precise synchronization, which often represents a technical challenge (Chanson, 2020). Herein, all data were synchronized based on the bore arrival time at the left tip of the reference probe (i.e., first air-to-water detection corresponded to $T = 0$), and the results were ensemble averaged or mediated over all available repetitions.

As shown in Table I, the present study was based on three main datasets, leading to the following methodology:

1. A detailed sensitivity analysis is conducted in Sec. IV based on dataset 1 (reference probe and 2000 repetitions at one elevation $z/d_1 = 1.06$), providing an indication of the number of repetitions needed for statistically meaningful results (i.e., not biased by the randomness of the process) in terms of air–water flow properties and residual error. However, results from this sensitivity analysis are only valid at the elevation of the reference probe, i.e., $z/d_1 = 1.06$.
2. Dataset 2 (center probe, $Fr_1 = 2.4$, and 100 repetitions at 20 elevations) and dataset 3 (center probe, $Fr_1 = 2.1$, and 100 repetitions at 2 elevations) were used to verify these findings, expanding previous results to different locations and for different flow conditions.
3. These results provided a detailed spatial and temporal distribution of the ensembled air–water flow properties in breaking bores. Thus, in Sec. V, the applicability of this methodology to unsteady flows is presented and discussed, giving an insight on the physical process in a breaking bore with $Fr_1 = 2.4$.

IV. SENSITIVITY ANALYSIS

Sensitivity analysis was applied to a number of physical properties in air–water flows, including the number of interfaces per run (Sec. IV A), the bubble chord time (Sec. IV B), and the void fraction (Sec. IV C), employing both single and linear threshold techniques. The objective herein is to discuss the variability of these properties for increasing the number of repetitions, defining the minimum values necessary to obtain results within a desired confidence interval.

A. Number of interfaces per run

An interface was detected every time 50% of the threshold between air and water was crossed, i.e., $v = 0.5 \cdot (v_{max} + v_{min})$. This definition was identical for both single and linear threshold techniques (Fig. 2). The probability distribution function (PDF) of the number of interfaces per run recorded for all 2000 repetitions of the right tip of the reference probe (dataset 1, $Fr_1 = 2.4$, and $z/d_1 = 1.06$) is given in Fig. 3(a). The data showed a smooth distribution, characterized by very close mean and median values. The range of interfaces detected per run ranged between $N_{min} = 1$ and $N_{max} = 77$ for the right tip, with a PDF characterized by a low level of skewness. A further analysis showed some good agreement between the PDF and the beta distribution, applied to model the behavior of random variables within intervals of finite length,

$$f(\chi, \alpha, \beta) = \frac{1}{B(\alpha, \beta)} \chi^{\alpha-1} (1-\chi)^{\beta-1}, \tag{3}$$

where $B(\alpha, \beta)$ is the beta function and α and β are two positive shape parameters describing the distribution. Although the beta distribution is defined in the interval $\chi \in [0,1]$, here the interval was linearly extended to $[1, N_{max}]$ [Fig. 3(a)]. The relationship between the mean, the variance of the distribution, and shape parameters generated a closed two-equation system that allowed us to uniquely identify the distribution for a given dataset,

$$\overline{N} = \frac{\alpha}{\alpha + \beta}, \tag{4}$$

$$[\text{st. dev}(N)]^2 = \frac{\alpha\beta}{(\alpha+\beta+1)(\alpha+\beta)}. \tag{5}$$

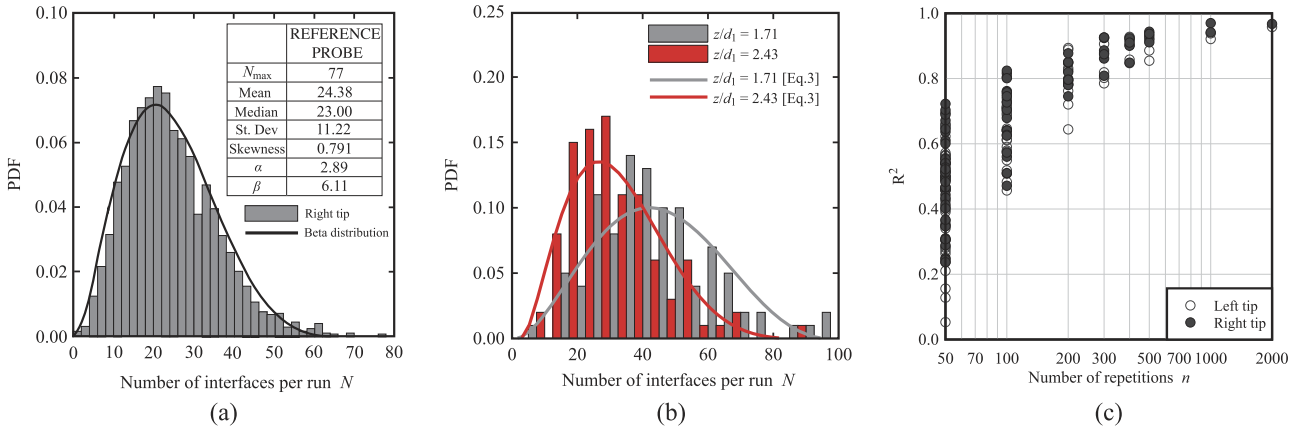

FIG. 3. (a) Probability distribution functions (PDFs) and basic statistical data of the number of interfaces per run recorded for the right tip of the reference probe (dataset 1: 2000 repetitions, $Fr_1 = 2.4$ at $z/d_1 = 1.06$); data are compared to the beta distribution in Eq. (3) with the interval extended to $[1, N_{max}]$ for a total of 48 762 interfaces. (b) PDFs of the number of interfaces per run recorded at two selected elevations (dataset 2: 100 repetitions per elevation, $Fr_1 = 2.4$). (c) Sensitivity analysis of the number of repetitions for comparison with the beta distribution in Eq. (3); analysis was performed for both tips of the reference probe at $z/d_1 = 1.06$, $Fr_1 = 2.4$ for 2000 repetitions (dataset 1). R^2 is the coefficient of determination between the dataset and the corresponding beta distribution.

A comparison between the PDF of the number of interfaces per run and the beta distribution was tested at various elevations within the bore roller, each based on 100 repetitions (dataset 2, Table I). Results for $Fr_1 = 2.4$ (dataset 2) at two selected elevations are represented in Fig. 3(b), where a relatively good agreement is observed, despite some scatter attributed to the lower number of repetitions available (i.e., $n = 100$) compared to the reference probe data (i.e., $n = 2000$).

The comparison with the beta distribution showed some good agreement for largest dataset 1 [reference probe, Fig. 3(a): 2000 repetitions for $Fr_1 = 2.4$] and a lesser agreement for dataset 2 with 100 repetitions [Fig. 3(b)]. This might suggest that for a full characterization of the distribution, 100 repetitions might not be sufficient. A sensitivity analysis in terms of the number of repetitions necessary to obtain a good representation of the beta distribution was attempted for $50 < n < 2000$ repetitions based on the data collected by the reference probe (dataset 1, $Fr_1 = 2.4$). For each non-overlapping sub-dataset, the coefficient of determination (i.e., the square of the normalized coefficient of correlation) R^2 between the data and the corresponding beta distribution was computed and plotted in Fig. 3(c) as a function of the number of repetitions n. The results hinted that a minimum of 200 repetitions was necessary to obtain $R^2 > 0.7$ and 300 for $R^2 > 0.8$.

To investigate the influence of the number of repetitions n on the ensemble-median number of interfaces per run N, dataset 1 (2000 repetitions) was subdivided into a number of non-overlapping sub-datasets, whose median values $\langle N \rangle$ are shown in Fig. 4, normalized by the ensemble-median value obtained for all 2000 repetitions $\langle N \rangle_{2000}$. The results for both tips of the reference probe showed that less than 20 repetitions yielded a high level of scatter, with values up to 2 or 3 times $\langle N \rangle_{2000}$. Little difference was observed for repetitions between 20 and 100, with an error within ±50%. A convergence toward $\langle N \rangle_{2000}$ was observed for $n > 100$ repetitions [Fig. 4(a)]. The same procedure was performed at different elevations for both $Fr_1 = 2.4$ and 2.1 in Figs. 4(b) and 4(c), respectively, showing a converging behavior toward the ensemble-median values for 100 repetitions.

The influence of the sampling frequency on the number of interfaces detected per run was also investigated. The raw signal (100 kHz) was sub-sampled, and the number of interfaces was computed for all non-overlapping segments. The results for the reference probe (dataset 1: 2000 repetitions, $Fr_1 = 2.4$ at $z/d_1 = 1.06$) were analyzed in terms of ensemble-median values. The data showed that a sampling frequency of 20 kHz only detected 95% of the interfaces detected at 100 kHz, pointing out the importance of higher sampling rates in highly unsteady flows (Fig. 5). The same sensitivity analysis was performed on the center probe (dataset 2, $Fr_1 = 2.4$) at selected elevations, ranging from $z/d_1 = 1.06$ to 2.85, and ensemble-averaged over 100 repetitions. The results showed that, at higher elevations, lower frequencies were able to capture the same number of interfaces, even for lower sampling rates (Fig. 5). This was probably linked to the higher void fractions and larger bubble sizes in the upper part of the roller, which made bubbles easier to detect, even at lower sampling frequencies. This was consistent with previous steady flow results by Wüthrich and Chanson (2014) for flat, horizontal stepped spillways with a slope of 22.5°. Current data were also compared to a sensitivity analysis performed on hydraulic jump data ($Fr_1 = 5.0$), showing similar results (Chanson, 2007b). The data for $Fr_1 = 2.4$ were compared to values obtained for $Fr_1 = 2.1$ with 100 repetitions at two locations $z/d_1 = 1.16$ mm and $z/d_1 = 1.68$ (Fig. 5). The results showed that, for a lower Froude number, a reduced acquisition frequency was responsible for a reduction in the total number of detected interfaces per run at lower elevations, thus confirming the importance of higher acquisition frequencies for weaker bores.

B. Bubble chord times

A sensitivity analysis on the number of repetitions needed to obtain consistent values of the median bubble chord time $\langle t_{ch} \rangle$ is shown in Fig. 6(a) for both tips of the reference probe, consisting of 2000 repetitions each (dataset 1: $Fr_1 = 2.4$, $z/d_1 = 1.06$). The total number of tests was subdivided into a number of non-overlapping segments, analyzed independently. Data in Fig. 6(a) showed that at $z/d_1 = 1.06$, a minimum of 10–20 repetitions was necessary to obtain an estimation of the median chord time within an error of ±50%. To reduce the error to ±20%, the number of repetitions had to be increased to at least 100. The same analysis was performed for the center probe at different elevations for $Fr_1 = 2.4$ [dataset 2: 100 repetitions per elevation, Fig. 6(b)] and $Fr_1 = 2.1$ [dataset 3: 100 repetitions per elevation, Fig. 6(c)], revealing similar behaviors.

C. Void fraction

The void fraction represents the probability of having air at a specific location (x, z) and time t, making it a function of both space and time: $c = f(x, z, t)$. In unsteady flows, the void fraction cannot be computed with the traditional time-average approach. Instead, an instantaneous value must be obtained through ensemble-statists based on multiple repetitions (Leng and Chanson, 2019b). The instantaneous void fraction data were characterized by two peaks at $c = 0$ (water) and $c = 1$ (air), presenting a strongly bimodal distribution with peaks at both ends, namely, a U-bimodal distribution according to Galtung (1969) "*AJUS*" classification. For these, the mean and median values have different values. Herein, the void fraction was estimated using both a single and a linear threshold technique, detailed in Secs. IV C 1 and IV C 2, respectively.

1. Single threshold technique

With a single threshold technique, the instantaneous void fraction c can be considered a discrete Bernoulli variable with two possible outcomes: $c = 0$ for air and $c = 1$ for water [Fig. 2(a)]. With each experiment being considered a Bernoulli trial, the influence of the number of repetitions on the estimation of the void fraction was tested. Similar approaches were previously used for blockage probability in hydraulic structures due to large wood debris, where statistical data are given by the total number of blocked stems over the total number of stems (Schalko, 2018; Furlan *et al.*, 2019). Herein, the ensemble-averaged instantaneous void fraction C, i.e., the maximum likelihood estimator that there will be air at that time and location, can be defined as the number of times the probe was in air ($n_{c=1}$) divided by the total number of repetitions n,

$$C(x, z, t) = \frac{n_{c=1}}{n}. \tag{6}$$

For the reference probe (dataset 1, $Fr_1 = 2.4$, and 2000 repetitions), a sensitivity analysis was developed in terms of the void

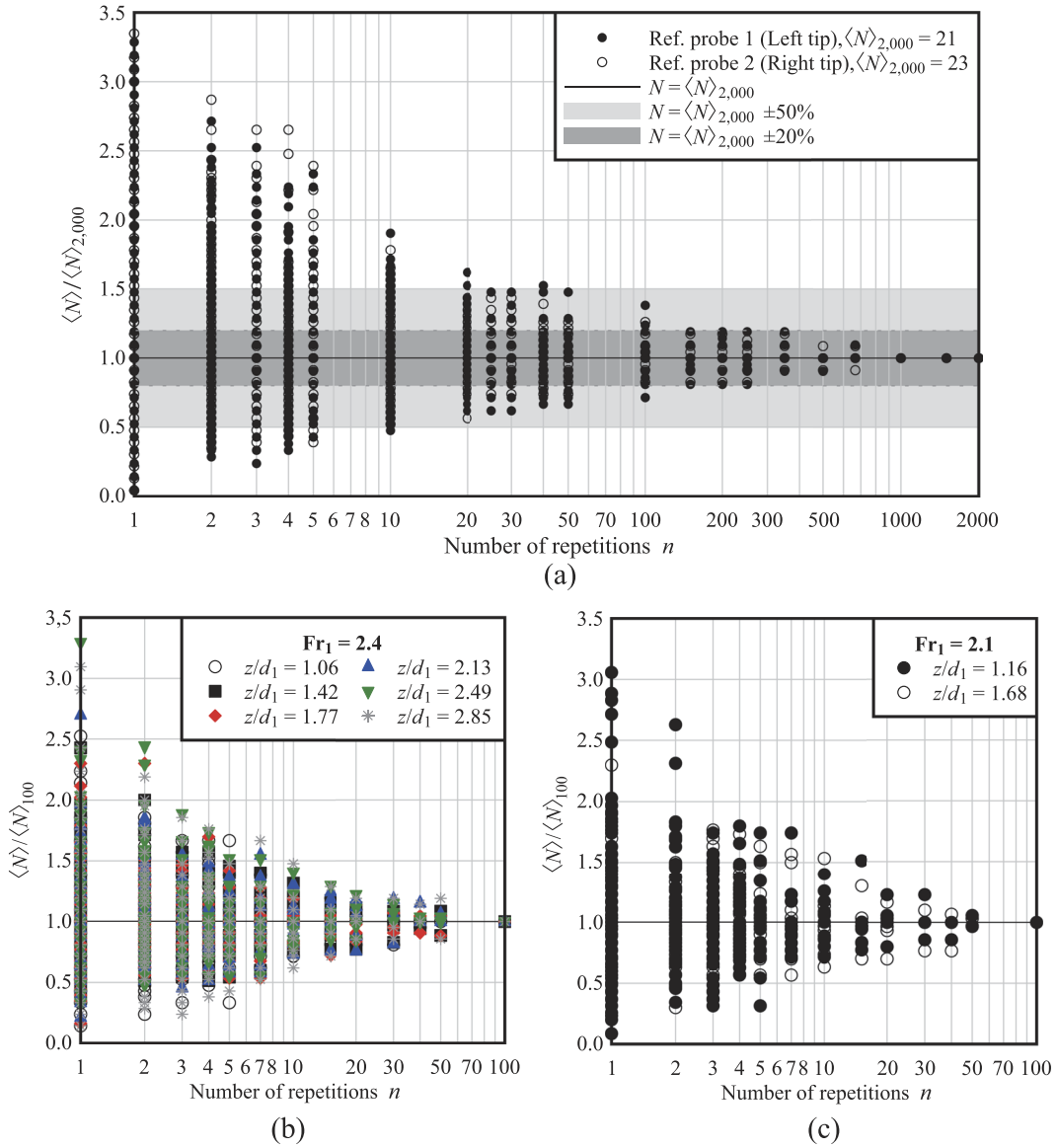

FIG. 4. Sensitivity analysis for the number of interfaces N detected per run: (a) reference probe (dataset 1: 2000 repetitions) for $Fr_1 = 2.4$ at $z/d_1 = 1.06$. (b) Center probe at six selected elevations (dataset 2: $Fr_1 = 2.4$, 100 repetitions). (c) Center probe at two elevations (dataset 3: $Fr_1 = 2.1$, 100 repetitions). Data are normalized using $\langle N \rangle_{2000}$ and $\langle N \rangle_{100}$, which are the ensemble-median value computed over 2000 and 100 runs, respectively.

fraction computed on a number of non-overlapping sub-samples of the signal, post-processed with a single threshold technique. The analysis was conducted for the left tip of the probe, and more data can be found in the work of Shi *et al.* (2021). The results are shown in Fig. 7 at $T = 0.025$ s, where $T = 0$ is the reference time, set when the first air-to-water interface was detected by the right tip of the reference probe. At this selected point, the complete dataset revealed ensemble-median void fraction $\langle C \rangle_{2000} = 0$ and ensemble-averaged $C_{2000} = 0.439$. The bimodal nature of the distribution showed that the use of the median was physically meaningless, as for a discrete series it only assumed values of 0 and 1. The application of Eq. (6) coincided with the use of an ensemble-averaged technique, and the data showed converging values for a minimum of 20 repetitions; however, the scatter remained important.

The variation of the ensemble-averaged void fraction C for a cumulative number of repetitions is represented in Fig. 8 at the same time $T = 0.025$ s behind the bore front (reference probe, dataset 1, $Fr_1 = 2.4$, and 2000 repetitions). As expected, results showed decreasing confidence intervals with an increasing number of repetitions.

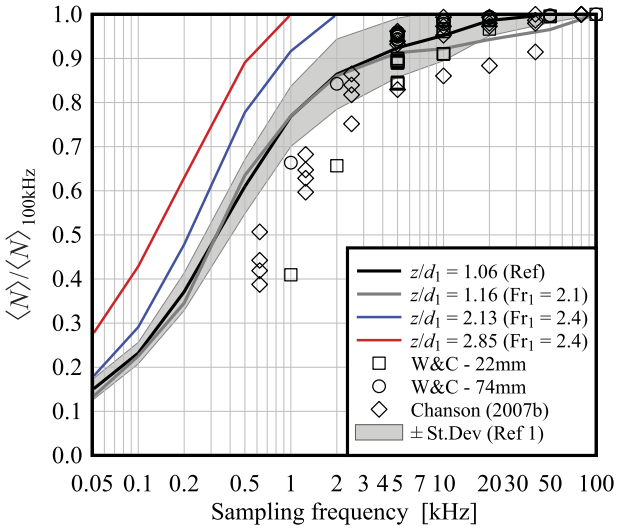

FIG. 5. Effect of sampling frequency on the number of interfaces per run: reference probe (dataset 1: 2000 repetitions, $Fr_1 = 2.4$, and $z/d_1 = 1.06$) and center probe at two selected elevations (dataset 2: center probe, 100 repetitions, and $Fr_1 = 2.4$) and comparison with data for $Fr_1 = 2.1$ at $z/d_1 = 1.16$ (dataset 3: center probe and 100 repetitions). Data are compared with those of Wüthrich and Chanson (2014) for a stepped spillway with a critical-depth/step-height of 1.3 at step-edge 10 and (Chanson, 2007b) for a hydraulic jump with $Fr_1 = 5.0$ ($d_1 = 0.029$ m, $Q = 0.019$ m^3/s).

The ensemble-averaged void fraction was highly varied for less than 30 repetitions, before stabilizing at $C \sim C_{2000}$.

The confidence intervals of the binomial distribution were computed, allowing us to further investigate their variability with the number of repetitions. A confidence interval states that, with a given level of "*certainty*," the true value will likely be in the identified range (Wallis, 2013). The lower confidence interval is denoted as L_L, and upper limit is denoted as U_L. The interval $[L_L; U_L]$ is associated with a confidence level of $100 \cdot (1 - \zeta)\%$, where ζ is the error level. The intervals are computed based on the sampling distribution of the instantaneous void fraction, and it will contain the value of the ensemble-averaged void fraction, $(1 - \zeta)$ percent of the times (Pires and Amado, 2008). These intervals depend on the number of independent trails and the method of calculation. In line with the work of Furlan *et al.* (2019), two methods are used herein to calculate confidence intervals:

1. Wald method (Appendix A), which calculates a symmetrical binomial confidence interval based on the approximation of the binomial distribution with the Normal distribution, and
2. Clopper–Pearson "*exact*" method (Appendix B), which is mathematically more complicated, but it was introduced to overcome the limitations of the Wald method (Clopper and Pearson, 1934).

The results are given in Fig. 8, with confidence intervals decreasing for the increasing number of repetitions, confirming that the Clopper–Pearson method produced wider confidence intervals, thus representing a more conservative approach (Clopper and Pearson, 1934; Agresti and Coull, 1998; and Sauro and Lewis, 2005).

For both Wald and Clopper–Pearson methods, the confidence interval (C.I.) was identified as C.I. = $U_L - L_L$ and plotted in Fig. 9(a) for two selected times behind the front, corresponding to different ensemble-averaged void fractions C_{2000}. The results showed that less than ten repetitions resulted in confidence intervals larger than ±0.22 (i.e., C.I. ≈ 0.45) and 50 repetitions to ±0.1 (i.e., C.I. ≈ 0.2). A minimum of ~100 repetitions were necessary to achieve a Clopper–Pearson C.I. of ±0.075 (i.e., C.I. = 0.15) with an 80% probability that the "*exact*" value might fall within this interval. The importance of this probability value is reflected in Fig. 9(b), showing that the same 100 repetitions would lead to a 50% confidence interval of ~0.08 and a 90% confidence interval of ~0.17. This clearly indicated the interplay between the extension of the confidence interval and its associated probability in the assessment of the void fraction in highly unsteady flows.

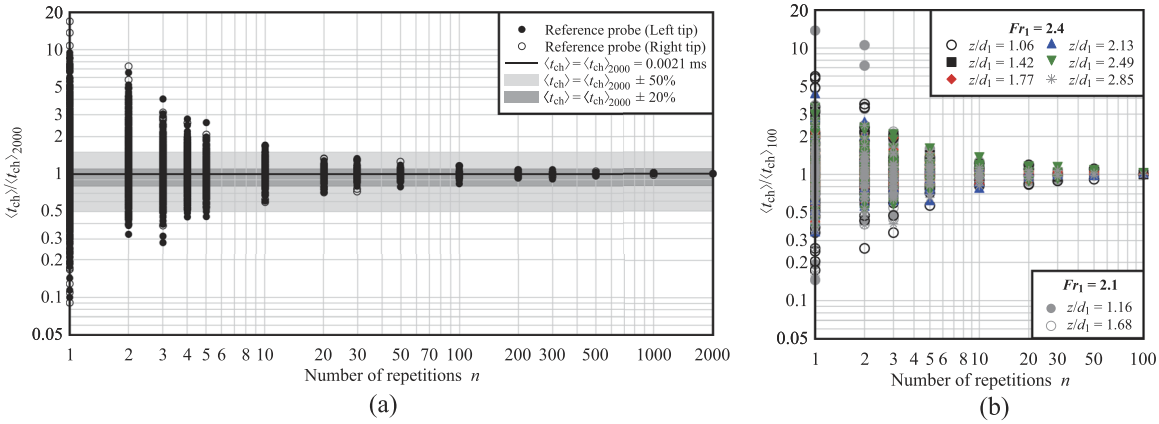

FIG. 6. Sensitivity analysis of the median chord time $\langle t_{ch} \rangle$ for (a) reference probe at a fixed elevation $z/d_1 = 1.06$ for 2000 repetitions, $Fr_1 = 2.4$ (dataset 1); (b) center probe at six elevations for $Fr_1 = 2.4$ (dataset 2), and two elevations for $Fr_1 = 2.1$ (dataset 3) based on 100 repetitions each.

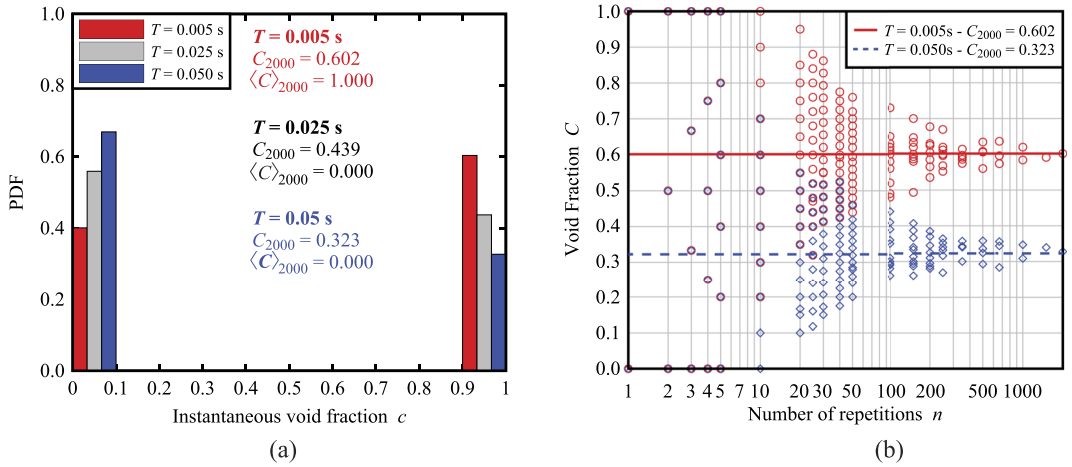

FIG. 7. Instantaneous void fraction data with single threshold technique at selected times behind the front: (a) PDF of the raw signal, with the ensemble-averaged C_{2000} and ensemble-median $\langle C \rangle_{2000}$ values. (b) Sensitivity analysis for the reference probe. Dataset 1 is given as follows: 2000 repetitions, $Fr_1 = 2.4$, and $z/d_1 = 1.06$ (Table I). Data refer to the left tip of the reference probe, while the right tip was used to synchronize all repetitions.

The results also showed that, for repetitions $n > 20$, lower void fractions ($T = 0.100$ s, $C_{2000} = 0.160$) were associated with smaller confidence intervals [Fig. 9(a)]. This finding hinted a relationship between void fraction and confidence intervals, visible in Fig. 9(c). The results showed a symmetrical pseudo-parabolic behavior for both methodologies, with a maximum at $C = 0.5$, indicating that the most uncertainties occurred for $0.4 < C < 0.6$. A simplified solution of the Clopper–Pearson confidence intervals was provided by Wüthrich *et al.* (2020a; 2020b) in Fig. 9(c) as a function of the C.I. at $C = 0.5$:

$$\frac{\text{C.I.}}{(\text{C.I.})_{C=0.5}} = 2 \cdot \sqrt{0.25 - (C - 0.5)^2}. \tag{7}$$

2. Linear threshold technique

The linear threshold technique applied to the raw signal is illustrated in Fig. 2(b). The raw voltage is associated with values of the instantaneous void fraction ranging across the interval $c \in [0; 1]$. That is, c is no longer a Bernoulli variable and the theory of discrete distributions does not apply. The ensemble-averaged instantaneous void fraction C, computed using the linear threshold technique to the 2000 repetitions of the left tip of the reference probe (dataset 1: $Fr_1 = 2.4$, $z/d_1 = 1.06$), is represented in Fig. 10(a) and compared to the corresponding single threshold technique. The data showed a decreasing void fraction trend with time from $C = 1$ (air) to $C = 0$ (water). With the exception of $0 < T < 0.015$ s, very little differences were observed between the linear and single threshold techniques. The results also suggested a substantial difference in behavior between the ensemble average and ensemble median, with the latter being characterized by a sudden decrease from $C = 1$ to $C = 0$ [Fig. 10(a)]. Herein, the ensemble-averaged void fraction was used as it was deemed more representative of the physical phenomenon. Results in terms of the Standard Error (SE) (Appendix A) showed a pseudo-parabolic shape, in line with the previous results

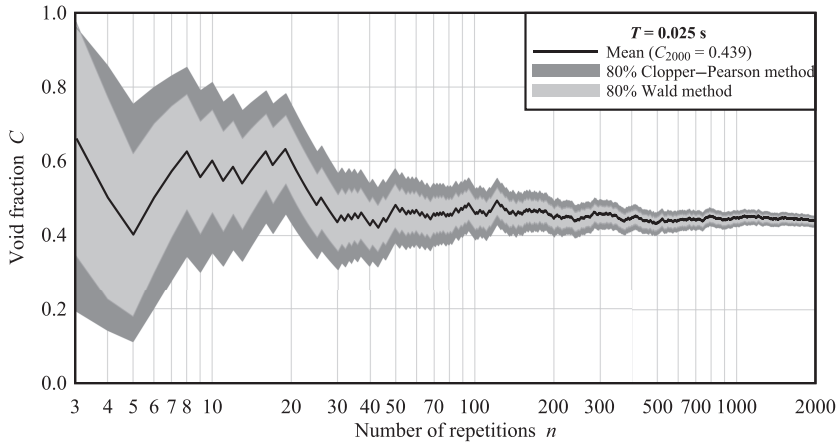

FIG. 8. 80% confidence intervals computed with Wald and Copper–Pearson methods at $T = 0.025$ s. Signal analyzed with a single threshold technique (dataset 1: left tip, $Fr_1 = 2.4$, $z/d_1 = 1.06$, and 2000 repetitions).

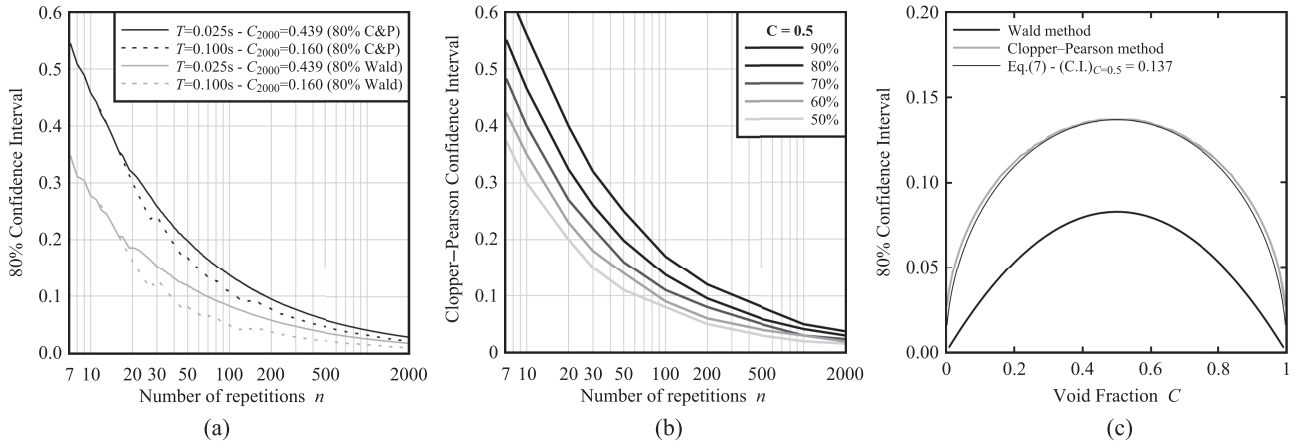

FIG. 9. (a) 80% confidence intervals for the void fraction obtained with a single threshold technique, computed with Wald and Copper–Pearson (C&P) methods at two selected times: $T = 0.025$ s ($C_{2000} = 0.439$) and $T = 0.100$ s ($C_{2000} = 0.160$) for the left tip of the reference probe (dataset 1: $Fr_1 = 2.4$, $z/d_1 = 1.06$, and 2000 repetitions). (b) Variability of the confidence intervals at $C = 0.5$ for various probabilities that the "*exact*" value might fall within this interval. (c) Same confidence intervals computed with Wald and Clopper–Pearson methods for a reduced number of 100 repetitions and plotted as a function of the void fraction C (dataset 1: $Fr_1 = 2.4$, $z/d_1 = 1.06$).

of Leng and Chanson (2019a). The linear threshold technique had some slightly smaller standard errors values compared to the single threshold technique [Fig. 10(b)].

Similarly to the single threshold technique (Fig. 7), the linear threshold technique resulted in a highly bimodal distribution of the instantaneous void fraction c, with peaks at the extremes of the interval, as shown in Fig. 11 for two selected times behind the bore front. These times are shown in Fig. 10(a) with vertical dashed lines. At $T = 0.005$ s and $T = 0.050$ s, a sensitivity analysis was conducted in terms of ensemble average C_{2000} as functions of the number of repetitions n (Fig. 11). In line with the results obtained for the single threshold technique, the use of the ensemble average seemed more appropriate, especially at large times, i.e., $C \to 0$, where the statistical approach using the ensemble average provided a better insight of the process [Fig. 10(a)]. Ensemble-averaged results showed substantial variations for less than 40 repetitions, while the data presented more constant values for more than 100 repetitions. The finding was consistent with the sensitivity analysis conducted for the

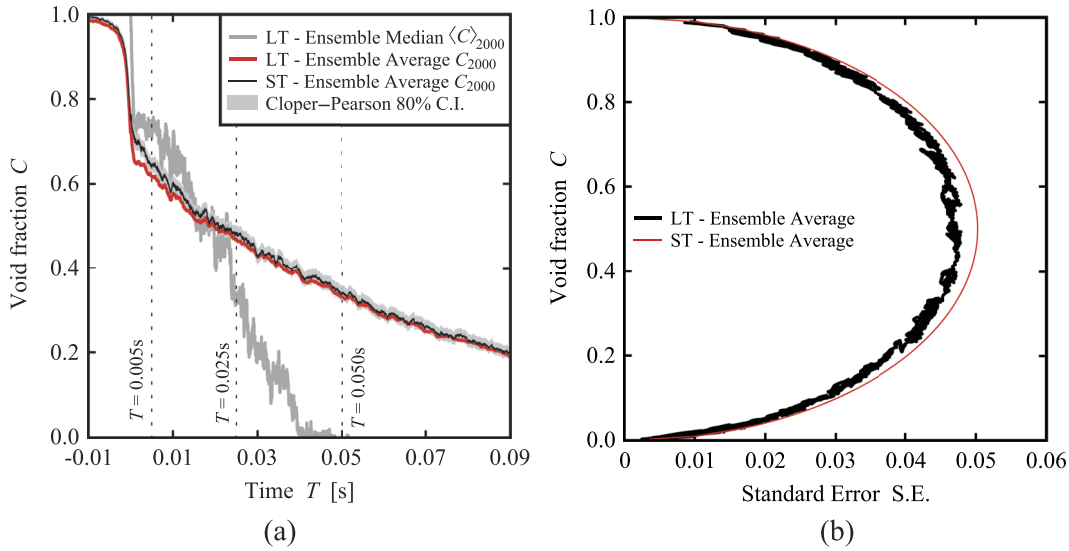

FIG. 10. (a) Temporal evolution of the void fraction data computed for the left tip of the reference probe using both single (ST) and linear (LT) threshold techniques, including a comparison between ensemble-median $\langle C \rangle_{2000}$ and ensemble-averaged C_{2000}; vertical dotted lines represent the selected times in Fig. 11. (b) Standard Error (SE) computed with Eq. (A2) and plotted as a function of the ensemble-averaged void fraction C for $T > 0$ s. All data refer to dataset 1: $Fr_1 = 2.4$, $z/d_1 = 1.06$, and 2000 repetitions.

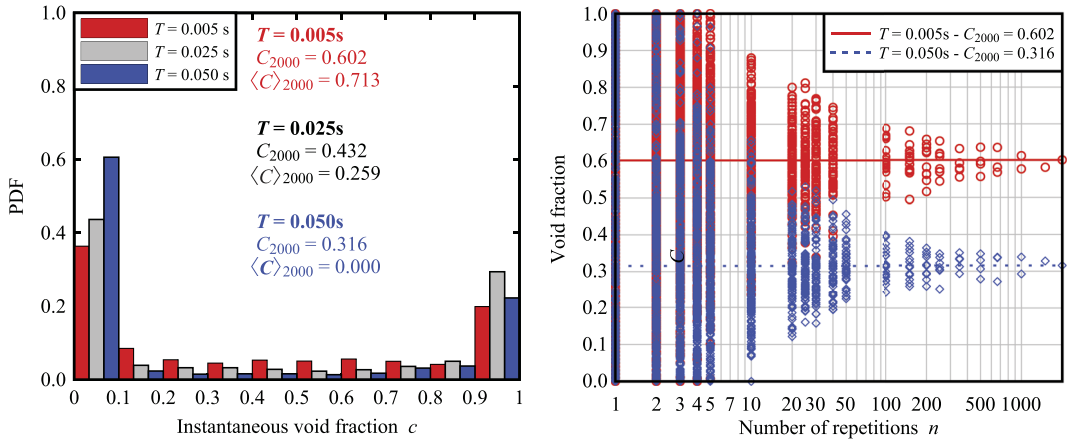

FIG. 11. Sensitivity analysis for the void fraction computed with the linear threshold technique at selected times behind the front: (a) PDF distribution of the instantaneous void fraction and (b) ensemble-averaged void fraction computed for increasing numbers of repetition. Data refer to dataset 1 with $Fr_1 = 2.4$, $z/d_1 = 1.06$ based on 2000 repetitions. Analysis was conducted for the left tip of the reference probe, as the right tip was used to synchronize all repetitions.

single threshold technique (Fig. 8), suggesting that a minimum of 40 repetitions is required for reliable void and liquid fraction values.

The same approach was applied for the center probe signal at difference elevations (dataset 2: $Fr_1 = 2.4$, 100 repetitions), when the ensemble-averaged void fraction $C_{100} = 0.5$, corresponding to the most uncertainty [Fig. 10(b)]. Although based on smaller datasets, these results revealed a similar behavior at all selected elevations (Fig. 12), thus suggesting that the results on the large dataset at $z/d_1 = 1.06$ could be extended to various elevations in the roller. Furthermore, these results in Fig. 12 confirmed that less than ten repetitions led to a high scatter and unreliable results, confirming the importance of large datasets when dealing with highly unsteady flows.

D. Sensitivity analysis: Concluding remarks

The objective of this sensitivity analysis was to assess the variability of the transient air–water flow properties in unsteady flows for the increasing number of repetitions. The study was based on 2000 repetitions at a single elevation ($z/d_1 = 1.06$) for one flow condition ($Fr_1 = 2.4$), conducted under ideal repeatability conditions. The results were then tested for smaller datasets of 100 repetitions at various elevations ($0.82 < z/d_1 < 2.85$) and flow conditions ($Fr_1 = 2.1$ and 2.4). Overall, this analysis revealed that the estimation of statistically meaningful air–water flow properties in highly unsteady flows, as well as the extension of their confidence intervals and residual error, highly depended on the number of repetitions and on the physical property that wants to be investigated. Based on the results presented in Secs. IV A, IV B, and IV C, a summary of the statistically justified minimum number of repetitions and residual error are presented in Table II for the main air–water flow properties, including the signal's acquisition frequency, the air–water interfaces, and the bubble chord time/lengths. For void fractions, the use of a single threshold technique (ST) allowed us to consider every run as a Bernoulli variable and, therefore, to develop the mathematically supported confidence interval (C.I.) based on the Clopper–Pearson "*exact*" methods. Practically, the C.I. will contain the ensemble-averaged void fraction $(1 - \zeta)\%$ of the times, providing an indication of the residual error. Examples of the extension of these confidence intervals for given probabilities $(1 - \zeta)\%$ are provided in Table II.

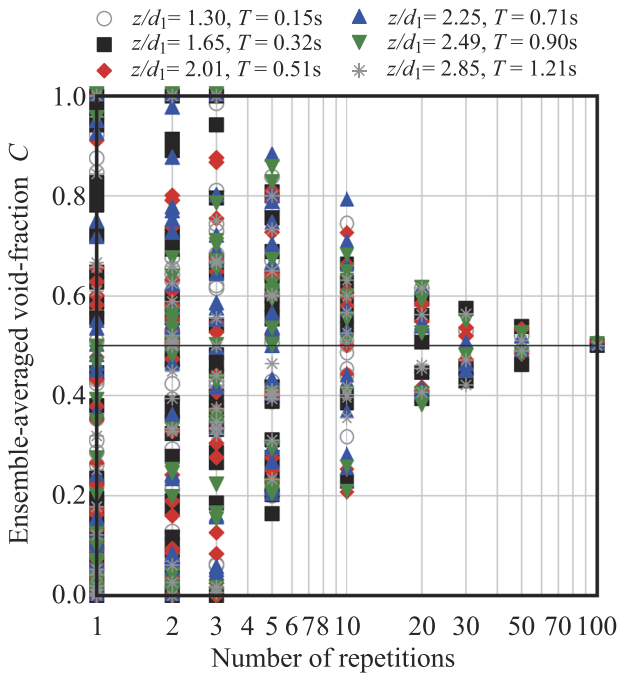

FIG. 12. Sensitivity analysis in terms of void fraction at six elevations when $C_{100} = 0.5$. Data refer to dataset 2 for the center probe with $Fr_1 = 2.4$ based on 100 repetitions.

TABLE II. Summary of the minimum number of repetitions needed for a given residual error, identified in the present study. Results based on 2000 repetitions at z/d_1 = 1.06 for Fr_1 = 2.4. Confidence intervals (C.Is.) were computed using the Clopper–Pearson "*exact*" method (Appendix B) and will contain the ensemble-averaged void fraction $(1 - \zeta)$% of the times (Pires and Amado, 2008). ST represents the single threshold technique.

	Error				
Parameter	50%	30%	20%	10%	Statistical operator
Signal's acquisition frequency	0.4 kHz	0.8 kHz	1.5 kHz	6 kHz	···
Air–water interfaces					
Number of interfaces per run	25	100	150	500	Median
Nature of the PDF[a]	100	200	300	1000	···
Bubble chord time	15	30	100	200	Median
Void fraction (ST)					
	$(1 - \zeta)$ = 50%	$(1 - \zeta)$ = 70%	$(1 - \zeta)$ = 80%	$(1 - \zeta)$ = 90%	
Single threshold – C.I. = 0.5	4	8	10	14	Average
Single threshold – C.I. = 0.3	10	18	24	36	
Single threshold – C.I. = 0.2	20	37	50	82	
Single threshold – C.I. = 0.1	70	138	189	338	

[a]Results in terms of R^2 between PDF and beta function. 50% : $R^2 > 0.5$; 20% : $R^2 > 0.8$; and 10% : $R^2 > 0.9$.

Altogether, more repetitions led to more accurate results and smaller confidence intervals. While, in practice, the maximum number of repetitions will likely be linked to time constraints, the amount to tests can be decreased if a lesser accuracy is acceptable. However, datasets with less than ten repetitions are not recommended, since all parameters investigated herein showed large scatter of the results and wide confidence intervals. As a general comment, it is acknowledged that the number of repetitions in experimental work is often affected by practical limitations and time availability, and thus, it is recommended to express the void fraction with its confidence interval and its level of confidence, as it remains a point estimator of an unknown quantity.

V. TRANSIENT AIR–WATER FLOW PROPERTIES IN A BREAKING ROLLER

This section presents the air–water flow properties obtained with dual-tip phase-detection probes located at the centerline, with ensemble results based on 100 repetitions at 20 elevations (dataset 2, Table I). In particular, the following parameters will be discussed: number of interfaces per run (Sec. V A), bubble chord time and lengths (Sec. V B), and void fraction (Sec. V C).

A. Number of interfaces per run

An interface was defined as a change in phase, i.e., either water-to-air or air-to-water. The ensemble-median number of interfaces per run N detected at the centerline is represented in Fig. 13 based on 100 repetitions per elevation. The results showed an increasing behavior for $z/d_1 < 1.77$, followed by a decreasing behavior in the upper region. A local maximum was observed at $z/d_1 \sim 1.65$, corresponding to the shear layer. The presence of this maximum is consistent with the bubble count rate data observed in the hydraulic jump's shear layer region (Chanson and Brattberg, 2000; Wang, 2014). At two elevations (z/d_1 = 1.16 and 1.68), the data for Fr_1 = 2.4 were also compared with breaking bore data for Fr_1 = 2.1 (100 repetitions), showing a similar number of interfaces for both Froude numbers. Current data were also compared with the previous data of Leng and Chanson (2019a) for a Froude number Fr_1 = 2.1 based on a single run, showing a relatively good agreement, despite the scatter associated with the lower number of repetitions (Fig. 13).

B. Bubble chord time and pseudo-chord length

For every bubble detected by the phase-detection probe sensor, its duration was extracted as the time difference between a water-to-air interface and the subsequent air-to-water interface. The statistical

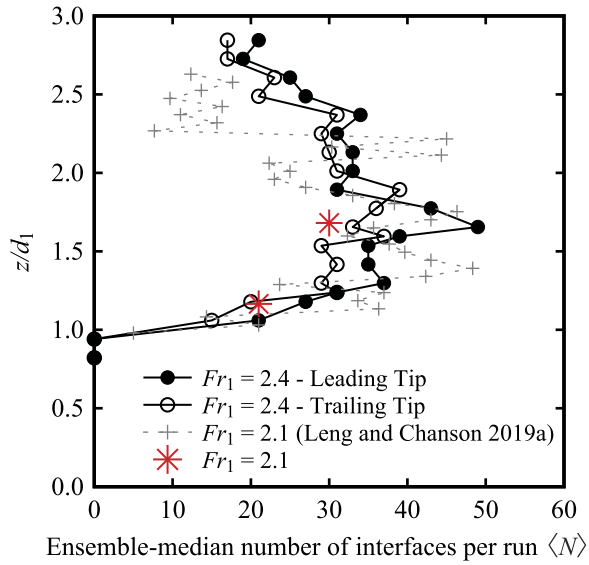

FIG. 13. Vertical distribution of the number of interfaces per run, ensemble-mediated over 100 repetitions $\langle N \rangle$. Data for both leading and trailing tips for Fr_1 = 2.4 were compared to Fr_1 = 2.1 for two elevations (z/d_1 = 1.16 and 1.68, 100 repetitions) and data from the work of Leng and Chanson (2019a), obtained for a single run, averaged over three probe tips.

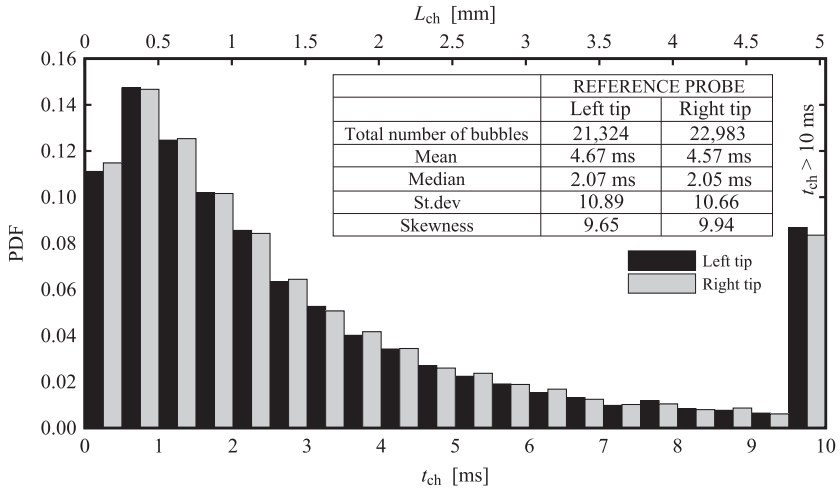

FIG. 14. PDF and main statistical data of the bubble chord times t_{ch} and pseudo-chord lengths $L_{ch} = U \cdot t_{ch}$ for both tips of the reference probe (dataset 1: Fr_1 = 2.4; z/d_1 = 1.06; U = 0.504 m/s; 2000 repetitions).

distributions of bubble chord times t_{ch} and pseudo-chord lengths $L_{ch} = U \cdot t_{ch}$ are represented in Fig. 14 for the reference probe (z/d_1 = 1.06) during 2000 repetitions. The results for both tips showed PDFs with similar behaviors, including a strong skewness, deviating from the Gaussian bell-shape and resulting in different values between mode, median, and mean. This is consistent with hydraulic jump data (Chanson, 2007a; Chachereau and Chanson, 2011), and the median was used for further analysis since this value was less affected by extreme values (Chanson, 2020). It is acknowledged that the intrusive nature of the phase-detection probes might affect the statistical distribution of the chord/length data, particularly for bubble sizes lesser than the probe's diameter. In addition, data also revealed a large number of outliers, here represented by t_{ch} > 10 ms.

Similarly, the PDFs of bubble chord times at selected elevations are represented in Fig. 15 based on 100 repetitions. In line with the reference probe, the PDFs revealed highly skewed distributions throughout the water depth, with a flattening pattern occurring for increasing elevations, i.e., an increase in standard deviation. In the upper part of the roller, the number of larger bubbles increased, possibly associated with the presence of entrapped air-pockets in the recirculating area. This confirmed the need to use ensemble-median values to limit the effect of these outliers. At two elevations (z/d_1 ~ 1.16 and 1.68), the statistical distributions of the bubble chord times for Fr_1 = 2.4 were compared with those obtained for Fr_1 = 2.1. The results showed similar behaviors in the lower part of the roller [z/d_1 ~ 1.15, Fig. 15(a)], while, in the upper part, the chord times for Fr_1 = 2.1 seemed to be slightly longer [Fig. 15(b)]. These datasets

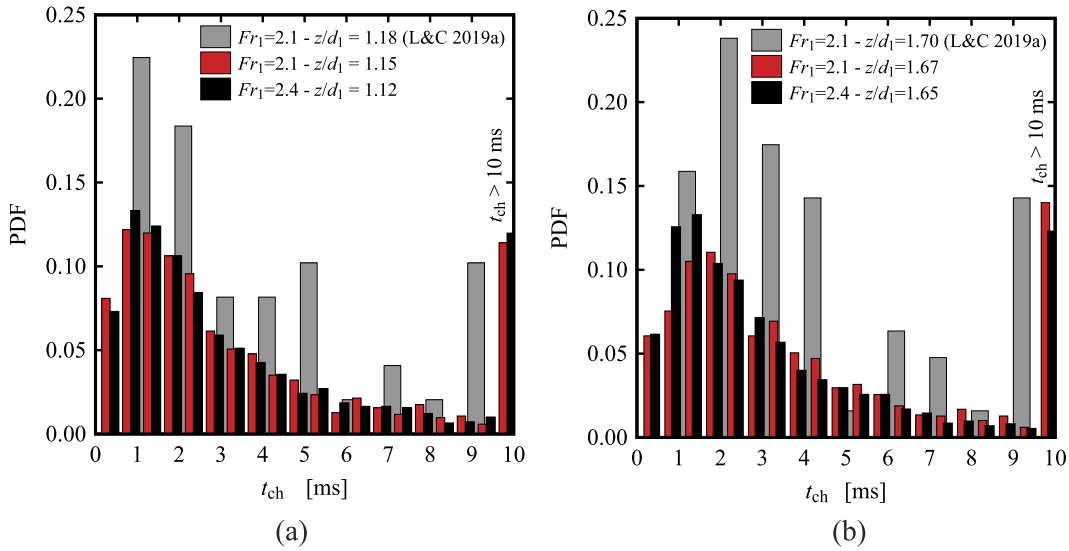

FIG. 15. PDF of the bubble chord time at different elevations and comparison between Fr_1 = 2.1 and 2.4: (a) Lower roller (1.12 < z/d_1 < 1.18). (b) Upper roller (1.65 < z/d_1 < 1.70). L&C (2019a) is data from the work of Leng and Chanson (2019a).

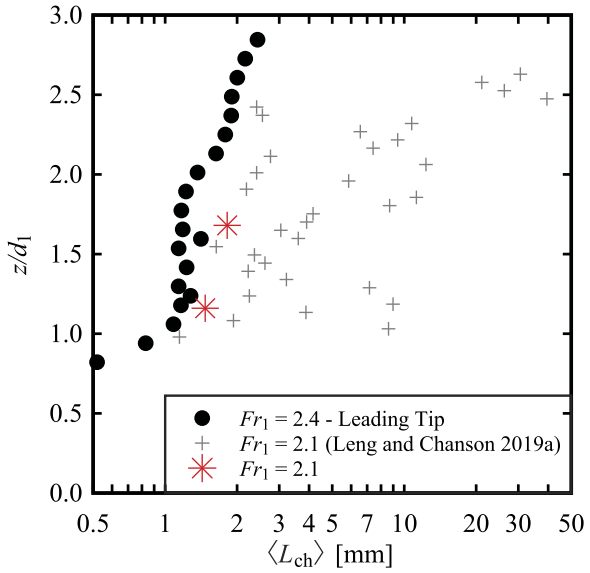

FIG. 16. Vertical distribution of median pseudo-chord length obtained from chord time as $L_{ch} = U \cdot t_{ch}$. Data for $Fr_1 = 2.4$ are computed as the median value over 100 repetitions. Data for $Fr_1 = 2.1$ (Leng and Chanson, 2019a) were obtained for a single run, averaged over three probe tips.

were also compared with previous data from the work of Leng and Chanson (2019a), showing similar values of the mode, despite the difference in the number of analyzed bubbles.

Vertical distributions of the median values of the chord lengths ($L_{ch} = U \cdot t_{ch}$) are represented in Fig. 16 based on 100 repetitions per elevation. A constant behavior with pseudo-chord lengths of ~1.2 mm was observed in the shear layer until $z/d_1 = 2$, followed by a constant increase in the upper recirculating zone, until the free-surface. The results for $Fr_1 = 2.4$ were also compared with data at two measurement locations for $Fr_1 = 2.1$, showing a relatively good agreement in terms of bubble chord time (Shi *et al.*, 2021). The results in terms of the pseudo-chord length in Fig. 16 revealed some larger values for $Fr_1 = 2.1$, attributed to the faster wave front celerity associated with the lower Froude number. For completeness, present data were also compared with previous results by Leng and Chanson (2019a), showing large differences in terms of both bubble chord time and pseudo-chord length, most likely attributed to the low number of repetitions.

C. Void fraction

The array of phase-detection probes allowed us to measure the instantaneous void fraction at 20 elevations in the range $0.82 < z/d_1 < 2.85$, with ensemble statistics based on 100 repetitions. The first air-to-water interface detected by the left tip of the reference probe was used to synchronize all repetitions, setting the time $T = 0$ s. The raw signal was post-processed using both single and linear threshold techniques, providing a value of the instantaneous void fraction for which $c = 0$ in water and $c = 1$ in air (Sec. III). As a result of the sensitivity analysis in Sec. IV C, only ensemble-averaged values were used to compute the void fraction. As expected, results showed a decrease in the void fraction from $C = 1$ (air) before the arrival of the bore to $C = 0$ (water) after the passage of the bore. An example of the void fraction data at six selected elevations is represented in Fig. 17(a). Despite some scatter, one can clearly notice milder slopes for increasing elevations, suggesting the presence of different diffusivity processes in the upper part of the roller. It is likely that these differences are associated with the effect of buoyancy on the bubbles raising from the lower part of the roller.

At eight selected times behind the bore front ($T = 0$ s), the void fraction profiles were identified and plotted as a function of elevation in Fig. 17(b). Both data obtained with single (ST) and linear (LT) thresholds techniques are presented with thick and thin lines, respectively, showing little differences between the two

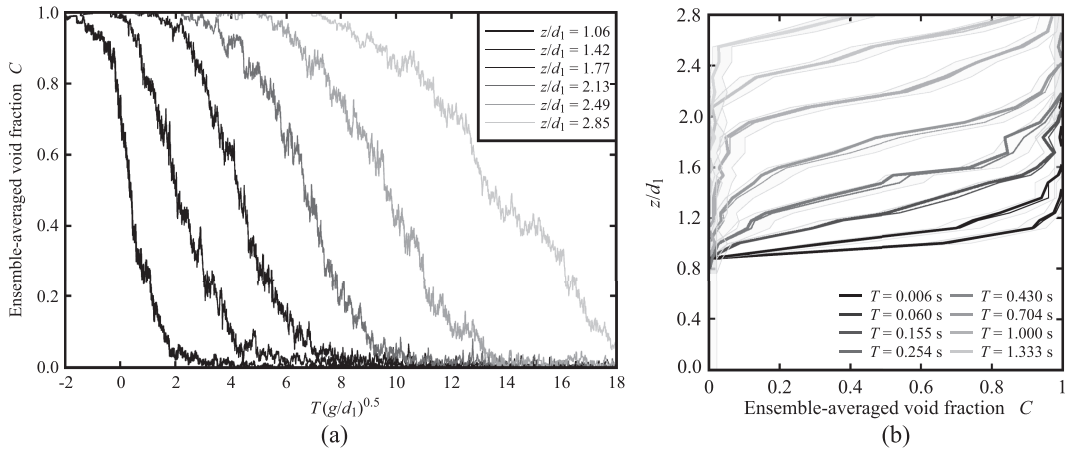

FIG. 17. (a) Behavior of the ensemble-averaged void fraction C as a function of time at six selected elevations of the roller's centerline (linear threshold technique) and (b) ensemble-averaged void fraction profiles at selected times behind the bore front ($T = 0$ s). Ensemble values are based on 100 repetitions. Note that Linear Threshold technique (LT) is the thick line and Single Threshold technique (ST) is the thin line, with gray shaded areas representing the Clopper–Pearson 80% confidence intervals (flow conditions: $Fr_1 = 2.4$, $\mathrm{Re} = 1.86 \times 10^5$, $d_1 = 0.084$ m, and $U = 0.504$ m/s).

methodologies. The Clopper–Pearson 80% confidence intervals were also computed from the single threshold data, revealing that for all profiles, the results obtained for the linear threshold technique were included within the confidence intervals. In terms of shape, results showed some convex profiles in the initial phases of the bore, i.e., for $T < 0.1$ s, in line with previous measurements on flash-flood surges on rough sloping channels (Chanson, 2004b; 2004c). For larger times, some typical *S*-shape profiles were observed, suggesting the absence of a lower shear layer, commonly observed in hydraulic jumps with similar Froude numbers (Wüthrich *et al.*, 2020b).

The void fraction profiles are compared in Fig. 18(a) with an analytical solution developed for the upper recirculating zone based on the advection-diffusion model. In particular, a theoretical solution [Eq. (8)] was developed by Shi *et al.* (2021) to describe the convex shape of the void fraction profiles, valid immediately downstream of the roller, for approximately $T \cdot U/d_1 < 0.6$,

$$C = 0.9\left(\frac{z - d_1}{z_{90} - d_1}\right)^M \quad \text{valid for} \quad T \cdot U/d_1 < 0.6, \tag{8}$$

where C is the ensemble-averaged void fraction, z is the vertical coordinate, z_{90} is the elevation where $C = 90\%$, d_1 is the upstream water depths, and M is an exponent such that $M = 0.9/C_{mean} - 1$, where C_{mean} is the depth-averaged air concentration computed between d_1 and z_{90}. Further downstream, for $T \cdot U/d_1 > 0.6$, the convex profiles modified into an *S*-shape [Fig. 18(a)], previously observed in hydraulic jumps and well approximated by Eq. (9), adapted from Chanson (2007a) for transient flows assuming $(x - x_{toe}) = U \cdot T$,

$$C = \frac{1}{2}\left[1 + \text{erf}\left(\frac{z - z_{50}}{2\sqrt{D^* \cdot \frac{U \cdot T}{V_1 + U}}}\right)\right] \quad \text{valid for} \quad T \cdot U/d_1 > 0.6, \tag{9}$$

where D^* is a diffusivity coefficient in the recirculation zone and z_{50} is the elevation where $C = 50\%$. Based on 100 repetitions at 20 elevations, for each instantaneous void-fraction profile, the best-fit values of D^* were computed and are represented in Fig. 18(b), showing a decreasing behavior as a function of time. With the assumption that $(x - x_{toe}) = U \cdot T$, the probe data were compared with an empirical expression proposed by Shi *et al.* (2021) derived through optical flow techniques near the sidewalls,

$$D^* = 0.014 \exp\left(-1.2 \cdot \frac{x - x_{toe}}{d_1}\right) + 0.0025. \tag{10}$$

The data from the conductivity probe showed similar diffusivity values to those derived with the optical flow techniques, thus confirming the validity of both approaches. Some differences were observed for $T \cdot U/d_1 < 0.6$, where Eq. (8) was shown to be more representative of the air–water exchange processes.

A contour map of void fraction data is represented in Fig. 19 for the leading tip of the center probe. Ensemble-averaged data based on 100 repetitions showed a smooth transition from $C = 1$ (air) to $C = 0$ (water) at all elevations. The data at the centerline are plotted against the acoustic displacement meter (ADM) data obtained at $x = 8.5$ m, ensemble-mediated over 25 repetitions. The results suggested that the ADM data followed the contour line $C = 0.7$, confirmed by the excellent agreement in Fig. 20(a) between ADM data and z_{70}, i.e., the elevation where $C = 0.7$. Similar results showing agreement between probe and ADM data were previously reported for breaking bores with $Fr_1 = 2.1$ (Leng and Chanson, 2019b), stationary hydraulic jumps (Chachereau and Chanson, 2011; Wang *et al.*, 2015), and in the skimming flow of stepped spillways (Felder, 2013).

From the void fraction vertical profiles, an instantaneous clear-water depth d is derived as

$$d = \int_{z=0}^{+\infty} (1 - C)\,dz, \tag{11}$$

where C is the ensemble-averaged void fraction and z is the vertical direction. This instantaneous clear-water depth d in unsteady flows was comparable with the equivalent clear-water depth commonly used in free-surface steady flows (Wood, 1985; 1984; and

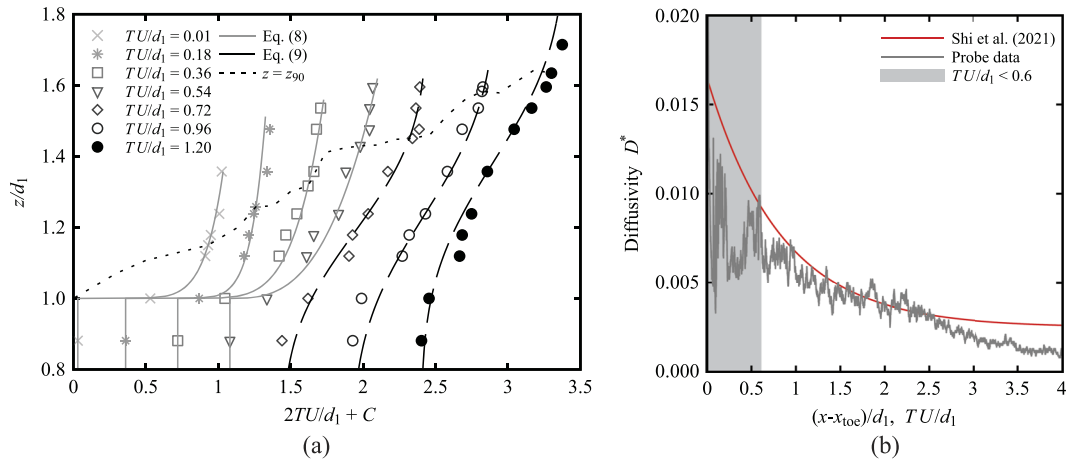

FIG. 18. (a) Comparison of void fraction profiles with theoretical models in Eqs. (8) and (9). (b) Variation of the diffusivity coefficient as a function of space and time. Note that it was assumed that $x - x_{toe} = T \cdot U$.

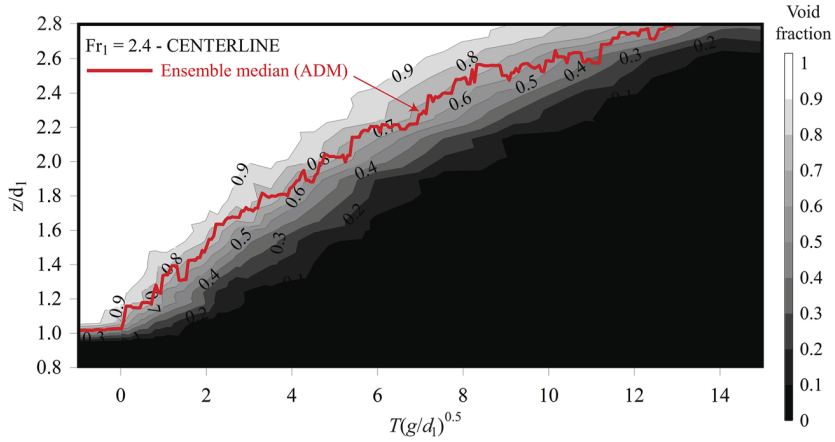

FIG. 19. Contour plot of the void fraction for the leading tip of the center probe (100 repetitions) and comparison with ADM data for Fr_1 = 2.4 at x = 8.5 m (ensemble median, 25 repetitions) (flow conditions: Fr_1 = 2.4, Re = 1.86 × 10^5, d_1 = 0.084 m, and U = 0.504 m/s).

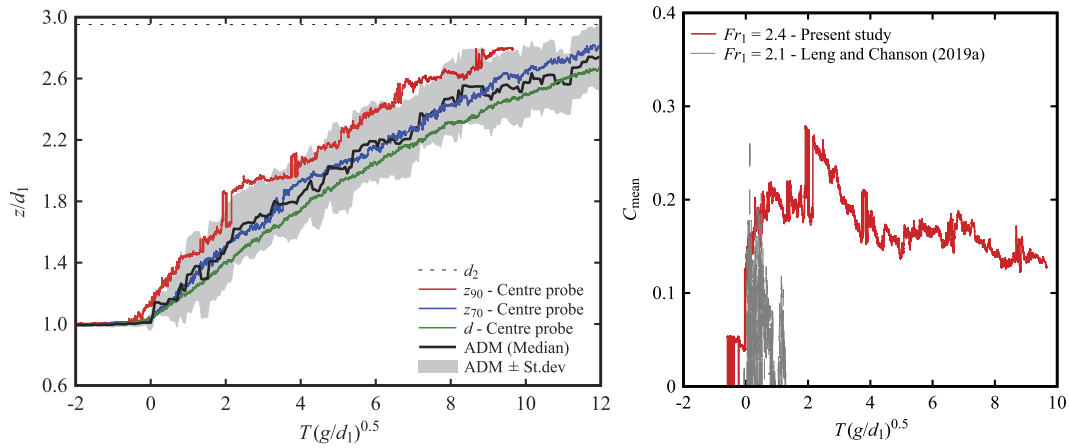

FIG. 20. (a) Comparison of roller profiles in terms of ADM data and phase-detection probe data z_{90}, z_{70} and clear-water depth d from Eq. (11). Gray shade represents the median value of ADM data ± st.dev (flow conditions: Fr_1 = 2.4, Re = 1.86 × 10^5, d_1 = 0.084 m, and U = 0.504 m/s). (b) Depth-averaged void fraction C_{mean} for a breaking bore with Fr_1 = 2.4. A comparison with the breaking bore with Fr_1 = 2.1 from the work of Leng and Chanson (2019a).

Chanson, 1997c). Values of the instantaneous clear-water depth d are compared to the bore profiles obtained with an acoustic displacement meter (ADM) in Fig. 20(a), systematically showing lower values than ADM data, but a behavior that was similar to z_{70}, i.e., the elevation where C = 0.7.

From the void fraction data, the depth-averaged air concentration C_{mean} was computed for each profile between z = 0 and $z = z_{90}$, i.e., the elevation at which C = 0.9,

$$C_{mean} = \frac{1}{z_{90}} \int_{z=0}^{z_{90}} C dz. \quad (12)$$

The results are shown in Fig. 20(b), showing an increasing behavior between $0 < T \cdot (g/d_1)^{0.5} < 2$ with a peak of approx. C_{mean} = 0.28. Then, a decreasing behavior was observed until $T \cdot (g/d_1)^{0.5} \approx 10$. Data for larger times could not be computed because z_{90} was outside of the measured range. A comparison with previous data from the work of Leng and Chanson (2019b) for a lower Froude number Fr_1 = 2.1 showed that while the maximum value was consistent for both studies ($C_{mean} \approx 0.28$), high scattering was recorded by Leng and Chanson (2019a), likely associated with the low number of repetitions and lesser air bubble entrainment for Fr_1 = 2.1.

VI. CONCLUSION

Air–water flow measurements in highly unsteady flows cannot rely on long-duration measurements. This represents a major limitation in the study of a number of environmental flows, including breaking waves, bores, storm surges, and tsunamis propagating inland. To fill this gap, a different approach is applied herein to investigate the air–water flow properties of breaking bores, compensating the lack of long-duration measurements with a large number of repetitions and analysis in terms of ensemble statistics. Based on a large experimental program obtained with an array of

two-phase-detection probes, this dataset included 2000 repetitions at a single elevation (reference probe) and 100 repetitions at 20 elevations for a bore with Fr_1 = 2.4 and 2 elevations for Fr_1 = 2.1. Herein, a detailed sensitivity analysis is presented in terms of the number of repetitions and sampling frequency necessary for reliable air–water flow properties, with examples of extension of the confidence intervals and residual errors summarized in Table II.

- Data for the *number of interfaces*, i.e., a phase change air-to-water or water-to-air, showed a random behavior best approximated by a beta distribution, with converging ensemble statistics for more than 20 repetitions and a residual error of 20% for 100 repetitions. The data also showed that an increase in sampling frequency from 20 to 100 kHz allowed us to capture about 5% more interfaces, particularly at lower elevations.
- *Bubble chord time/length* data showed highly skewed PDFs, affected by extreme values, thus recommending the use of the median for ensemble statistics. Sensitivity analysis showed that a minimum of 15 repetitions was necessary to obtain a median chord time within the 50% error and 100 for 20% error.
- The *void fraction* is the probability of having air at a specific location and time. The use of single and linear threshold techniques to convert the raw signal revealed air–water data characterized by a highly bimodal distribution with peaks at both ends. The binary nature of the single threshold technique allowed us to consider every run as a Bernoulli variable and to develop mathematically supported confidence intervals based on the Wald and Clopper–Pearson "*exact*" methods. Datasets with less than ten repetitions revealed large scatter of the results and wide confidence intervals. As expected, these decreased with the increasing number of repetitions, showing that 100 runs were needed for a characterization of void fractions with 80% Clopper–Pearson confidence intervals of 0.15, thus, adopted herein.

This methodology was then applied to the investigation of air–water flow properties in a breaking bore with Fr_1 = 2.4. The ensemble-median number of interfaces per run exhibited a *C*-shaped distribution, with the maximum value in the developing shear layer. The chord time data exhibited a right skewed distribution, in which over 90% of detected bubbles experienced a chord time less than 20 ms. Ensemble-averaged void fraction profiles were obtained at various times behind the front, showing convex profiles immediately downstream of the roller, followed by *S*-shaped profiles that compared well with theoretical solutions of the advection-diffusion model in hydraulic jumps and plunging jets. Contour plots of the void fraction data provided a comprehensive characterization of the presence of air within the breaking roller, revealing excellent agreement with acoustic water-depth measurements at 70% void fraction and equivalent clear-water depths. The computation of the depth-averaged mean air concentration revealed an increasing trend behind the roller, with a peak of ~0.28, followed by a decreasing behavior, in line with previous observations on stationary hydraulic jumps.

Overall, this methodology allowed us to capture the key transient air–water flow properties of breaking bores, going beyond the limitations imposed by the unsteady nature of the flow. This study showed results that were consistency with previous findings, hinting similarities with stationary hydraulic jumps for similar flow conditions. Nevertheless, it pointed out the need for more detailed investigation of transient air–water flow properties under different unsteady flows for a more complete understanding of the whole physical process.

ACKNOWLEDGMENTS

The authors acknowledge the helpful comments of Dr. Hubert Branger (University of Marseille), Dr. Xinqian (Sophia) Leng (University of Bordeaux), Professor Nobuhito Mori (Kyoto University), and Dr. Hang Wang (Sichuan University), as well as the technical assistance of Jason Van Der Gevel and Stewart Matthews (The University of Queensland, Australia).

The present study was funded by the Swiss National Science Foundation (Grant No. P2ELP2_181794) and the School of Civil Engineering at the University of Queensland (Australia).

AUTHOR DECLARATIONS

Conflict of Interest

The authors have no conflicts to disclose.

DATA AVAILABILITY

The data that support the findings of this study are available from the corresponding author upon reasonable request.

APPENDIX A: WALD METHOD

The Wald method calculates symmetrical binomial confidence intervals based on the approximation of the binomial distribution with the normal distribution,

$$C - c_{\zeta/2}\sqrt{\frac{C(1-C)}{n}} \leq C \leq C + c_{\zeta/2}\sqrt{\frac{C(1-C)}{n}}, \quad \text{(A1)}$$

where C is the void fraction and $c_{\zeta/2}$ denotes the $1 - \zeta/2$ quantile of the standard normal distribution (Vollset, 1993; Agresti and Coull, 1998). The term

$$SE = \sqrt{\frac{C(1-C)}{n}} \quad \text{(A2)}$$

is the Standard Error (SE) of the ensemble-averaged void fraction C. Figure 21 shows the evolution of the standard error at four selected times behind the front (dataset 1, Fr_1 = 2.14, z/d_1 = 1.06, and 2000 repetitions), where one can notice a decreasing behavior for an increasing number of repetitions. The confidence interval computed with Eq. (A1) was presented in Fig. 8 for the cumulative number of repetitions.

The Wald method presents, however, three major limitations: (1) when C tends to either 0 or 1, the product $C(1 - C)$ tends to 0, leading to an underestimation of the error; (2) the limits of the confidence intervals can exceed the interval [0,1]; and (3) it makes the assumption that the dataset follows a normal distribution (Agresti and Coull, 1998; Wallis, 2013), which is not correct in the present scenario, as shown in Fig. 7.

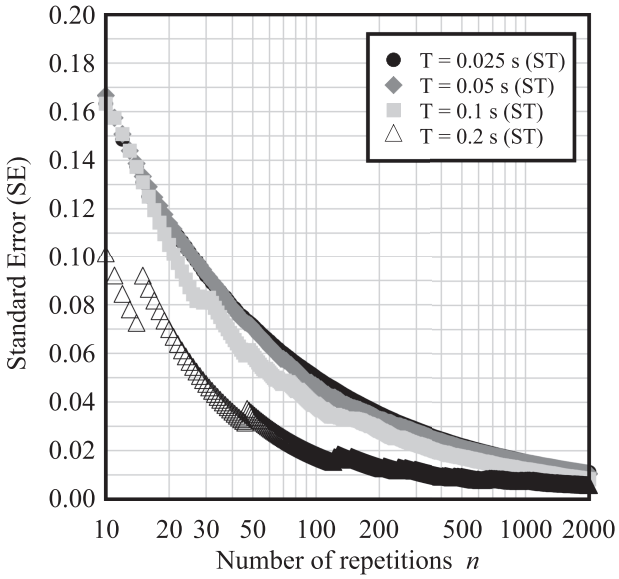

FIG. 21. Evolution of the standard error at four selected times behind the bore front, corresponding to different values of the void fraction (dataset 1, $Fr_1 = 2.14$, $z/d_1 = 1.06$, and 2000 repetitions). ST = Single Threshold technique.

APPENDIX B: CLOPPER–PEARSON METHOD

The Clopper–Pearson method (Clopper and Pearson, 1934) was introduced to overcome the limitations of the Wald method. It requires to solve the following equations:

$$\begin{aligned}\sum_{k=x}^{n}\binom{n}{k}{L_L}^k(1-L_L)^{n-k}&=\zeta',\\ \sum_{k=0}^{x}\binom{n}{k}{U_L}^k(1-U_L)^{n-k}&=\zeta'',\end{aligned}\tag{B1}$$

where $\zeta' + \zeta'' = 1$. The particular case $\zeta' = \zeta'' = 0.5$ gives the central exact interval. The Clopper–Pearson intervals can be rewritten as

$$\left[1+\frac{n-x+1}{xF_{2x,2(n-x+1),1-\zeta/2}}\right]^{-1} < C < \left[1+\frac{n-x}{(x+1)F_{2(x+1),2(n-x),\zeta/2}}\right]^{-1},\tag{B2}$$

where $F_{a1,a2,a3}$ is the $1 - a_3$ quartile of the F distribution with degrees of freedom a_1 and a_2. Herein, the confidence interval was computed for a number of repetitions ranging from 3 to 2000 using the Matlab toolbox *binofit*(χ, n, ζ), where χ is the number of successes (signal in air), n is the total number of repetitions, and ζ is a parameter that returns the $100 \cdot (1 - \zeta)$% confidence intervals, herein set to 80% to provide a meaningful comparison with the difference between the first and last decile of classical statistical distributions.

REFERENCES

Agresti, A. and Coull, B. A., "Approximate is better than 'exact' for interval estimation of binomial proportions," Am. Stat. **52**(2), 119–126 (1998).

Blenkinsopp, C. E. and Chaplin, J. R., "Void fraction measurements in breaking waves," Proc. R. Soc. A **463**(2088), 3151–3170 (2007).

Blenkinsopp, C. E. and Chaplin, J. R., "Void fraction measurements and scale effects in breaking waves in freshwater and seawater," Coastal Eng. **58**(5), 417–428 (2011).

Bradshaw, P., *An Introduction to Turbulence and Its Measurement, The Commonwealth and International Library of Science and Technology Engineering and Liberal Studies (Thermodynamics and Fluid Mechanics Division)* (Pergamon Presss, Oxford, 1971), p. 218.

Brattberg, T., Chanson, H., and Toombes, L., "Experimental investigations of free-surface aeration in the developing flow of two-dimensional water jets," J. Fluids Eng. **120**(4), 738–744 (1998).

Bullock, G. N., Crawford, A. R., Hewson, P. J., Walkden, M. J. A., and Bird, P. A. D., "The influence of air and scale on wave impact pressures," Coastal Eng. **42**(4), 291–312 (2001).

Cartellier, A., "Simultaneous void fraction measurement, bubble velocity, and size estimate using a single optical probe in gas–liquid two-phase flows," Rev. Sci. Instrum. **63**(11), 5442–5453 (1992).

Cartellier, A. and Achard, J. L., "Local phase detection probes in fluid/fluid two-phase flows," Rev. Sci. Instrum. **62**(2), 279–303 (1991).

Chachereau, Y. and Chanson, H., "Bubbly flow measurements in hydraulic jumps with small inflow Froude numbers," Int. J. Multiphase Flow **37**(6), 555–564 (2011).

Chang, K.-A., Lim, H.-J., and Su, C. B., "Fiber optic reflectometer for velocity and fraction ratio measurements in multiphase flows," Rev. Sci. Instrum. **74**(7), 3559–3565 (2003).

Chanson, H., *Air Bubble Entrainment in Free-Surface Turbulent Shear Flows* (Academic Press, London, 1997a), p. 401.

Chanson, H., "Air bubble entrainment in open channels. Flow structure and bubble size distributions," Int. J. Multiphase Flow **23**(1), 193–203 (1997b).

Chanson, H., "Measuring air-water interface area in supercritical open channel flow," Water Resour. **31**(6), 1414–1420 (1997c).

Chanson, H., "Comments on 'Fiber optic reflectometer for velocity and fraction ratio measurements in multiphase flows' [Rev. Sci. Instrum. 74, 3559 (2003)]," Rev. Sci. Instrum. **75**(1), 284–285 (2004a).

Chanson, H., "Experimental study of flash flood surges down a rough sloping channel," Water Resour. Res. **40**(3), W03301, https://doi.org/10.1029/2003wr002662 (2004b).

Chanson, H., "Unsteady air-water flow measurements in sudden open channel flows," Exp. Fluids **37**(6), 899–909 (2004c).

Chanson, H., "Bubbly flow structure in hydraulic jump," Eur. J. Mech.: B/Fluids **26**(3), 367–384 (2007a).

Chanson, H., "Dynamic similarity and scale effects affecting air bubble entrainment in hydraulic jumps," in Proceedings of the 6th International Conference on Multiphase Flow (ICMF 2007), Leipzig, Germany, July 9–13, 2007b.

Chanson, H., *Tidal Bores, Aegir, Eagre, Mascaret, Pororoca: Theory and Observations* (World Scientific, Singapore, 2011), p. 220.

Chanson, H., "Statistical analysis method for transient flows—The dam-break case," J. Hydraul. Res. **58**(6), 1001–1004 (2020).

Chanson, H. and Felder, S., "Turbulence measurements in air-water self-aerated flows: Basic analysis and results," in 7th International Conference on Multiphase Flow (ICMF 2010), Tampa, FL, 30 May–5 June 2010.

Chanson, H. and Toombes, L., "Experimental study of gas-liquid interfacial properties in a stepped cascade flow," Environ. Fluid Mech. **2**(3), 241–263 (2002).

Chanson, H. and Brattberg, T., "Experimental study of the air-water shear flow in a hydraulic jump," Int. J. Multiph. Flow **26**(4), 583–607 (2000).

Clopper, C. J. and Pearson, E. S., "The use of confidence or fiducial limits illustrated in the case of the binomial," Biometrika **26**(4), 404–413 (1934).

Cox, D. T. and Shin, S., "Laboratory measurements of void fraction and turbulence in the bore region of surf zone waves," J. Eng. Mech. **129**(10), 1197–1205 (2003).

Docherty, N. J. and Chanson, H., "Physical modelling of unsteady turbulence in breaking tidal bores," J. Hydraul. Eng. **138**(5), 412–419 (2012).

Felder, S., "Air-water flow properties on stepped spillways for embankment dams: Aeration, energy dissipation and turbulence on uniform, non-uniform and pooled stepped chutes," Ph.D. thesis, School of Civil Engineering, The University of Queensland, Brisbane, Australia, 2013.

Furlan, P., Pfister, M., Matos, J., Amado, C., and Schleiss, A. J., "Experimental repetitions and blockage of large stems at ogee crested spillways with piers," J. Hydraul. Res. **57**(2), 250–262 (2019).

Galtung, J., *Theory and Methods in Social Research* (Universitetsforlaget, Oslo, 1969).

Gonzalez, C. A., "An experimental study of free-surface aeration on embankment stepped chutes," Ph.D. thesis, Department of Civil Engineering, The University of Queensland, Brisbane, Australia, 2005.

Hoque, A. and Aoki, S. I., "Distributions of void fraction under breaking waves in the surf zone," Ocean Eng. **32**(14–15), 1829–1840 (2005).

Kimmoun, O. and Branger, H., "A particle image velocimetry investigation on laboratory surf-zone breaking waves over a sloping beach," J. Fluid Mech. **588**, 353–397 (2007).

Leng, X. and Chanson, H., "Unsteady turbulence, dynamic similarity and scale effects in bores and positive surges," Eur. J. Mech.: B/Fluids **61**, 125–134 (2017).

Leng, X. and Chanson, H., "Air-water interaction and characteristics in breaking bores," Int. J. Multiphase Flow **120**(3), 103101 (2019a).

Leng, X. and Chanson, H., "Two-phase flow measurements of an unsteady breaking bore," Exp. Fluids **60**(3), 42 (2019b).

Mori, N. and Kakuno, S., "Aeration and bubble measurements of coastal breaking waves," Fluid Dyn. Res. **40**(7–8), 616 (2008).

Na, B., Chang, K. A., Huang, Z. C., and Lim, H. J., "Turbulent flow field and air entrainment in laboratory plunging breaking waves," J. Geophys. Res.: Oceans **121**(5), 2980–3009, https://doi.org/10.1002/2015jc011377 (2016).

Pires, A. M. and Amado, C., "Interval estimators for a binomial proportion: Comparison of twenty methods," REVSTAT-Stat. J. **6**(2), 165–197 (2008).

Sauro, J. and Lewis, J. R., "Estimating completion rates from small samples using binomial confidence intervals: Comparisons and recommendations," Proc. Human Factors Ergon. Soc. Annu. Meet. **49**(24), 2100–2103 (2005).

Schalko, I., "Modelling hazards related to large wood in rivers," Ph.D. thesis, ETH Zürich, Switzerland, 2018, p. 208.

Schlichting, H. and Gersten, K., *Boundary-Layer Theory*, 8th ed. (Springer, Berlin, Germany, 2001), p. 707.

Shi, R., Wüthrich, D., and Chanson, H., "Air-water characteristics of a breaking bore roller Part II: Air-water flow properties," in *Hydraulic Model Report No. CH118/21*, School of Civil Engineering, The University of Queensland, Brisbane, Australia, 2021, p. 159.

Tricker, R. A. R., *Bores, Breakers, Waves and Wakes* (American Elsevier Publishing Company, New York, 1965).

Vollset, S. E., "Confidence intervals for a binomial proportion," Stat. Med. **12**(9), 809–824 (1993).

Wallis, S., "Binomial confidence intervals and contingency tests: Mathematical fundamentals and the evaluation of alternative methods," J. Quant. Linguist. **20**(3), 178–208 (2013).

Wang, H., "Turbulence and air entrainment in hydraulic jumps," Ph.D. thesis, School of Civil Engineering, The University of Queensland, Brisbane, Australia, 2014, p. 341 and Digital Appendices.

Wang, H., Murzyn, F., and Chanson, H., "Interaction between free-surface, two-phase flow and total pressure in hydraulic jump," Exp. Therm. Fluid Sci. **64**, 30–41 (2015).

Wüthrich, D. and Chanson, H., "Aeration and energy dissipation over stepped Gabion spillways: A physical study," in *Hydraulic Model Report No. CH92/13*, School of Civil Engineering, The University of Queensland, Brisbane, Australia, 2014, p. 171.

Wüthrich, D., Shi, R., and Chanson, H., "Air-water flow properties in breaking bores and stationary hydraulic jumps with similar Froude number-analogies and dissimilarities," in Proceedings of the 8th IAHR International Symposium on Hydraulic Structures ISHS2020, Santiago, Chile, 12–15 May 2020a.

Wüthrich, D., Shi, R., and Chanson, H., "Sensitivity analysis in air-water measurements under highly unsteady flow conditions," in 22nd Australasian Fluid Mechanics Conference AFMC2020, Brisbane, Australia, 7–10 December 2020b.

Wüthrich, D., Pfister, M., Nistor, I., and Schleiss, A. J., "Experimental study on the hydrodynamic impact of tsunami-like waves against impervious free-standing buildings," Coast. Eng. **60**(2), 180–199 (2018).

Wood, I., "Air entrainment in high speed flows," in *Symposium on Scale Effects in Modelling Hydraulic Structures IAHR*, paper 4.1, edited by Kobus, H., Esslingen, Germany (IAHR, 1985), p. 7.

Wood, I. R., "Air water flows," in *Proceedings of the 21st IAHR Congress,* Melbourne, Australia, Keynote address (1985) pp. 18-29.